photonics

Communication

Coupling of Photonic and Plasmonic Modes for Double Nanowire Cavities

Xuanran Peng [1,2,3], Jing Liu [1,2,3], Yaru Kang [1,4], Xu Mao [1], Wei Yan [1,*], Xiaohui Wang [2,5], Kong Liu [2,5], Rui Xu [6], Fuhua Yang [1,2,3,7,8,9] and Zhaofeng Li [1,2,4,*]

1 Engineering Research Center for Semiconductor Integrated Technology, Institute of Semiconductors, Chinese Academy of Sciences, Beijing 100083, China
2 Center of Materials Science and Optoelectronics Engineering, University of Chinese Academy of Sciences, Beijing 100049, China
3 College of Materials Science and Opto-Electronics Technology, University of Chinese Academy of Sciences, Beijing 100049, China
4 School of Integrated Circuits, University of Chinese Academy of Sciences, Beijing 100049, China
5 Key Laboratory of Semiconductor Materials Science, Beijing Key Laboratory of Low Dimensional Semiconductor Materials and Devices, Institute of Semiconductors, Chinese Academy of Sciences, Beijing 100083, China
6 Fachgebiet Angewandte Nanophysik, Institut für Physik & IMN MacroNano, Technische Universität Ilmenau, 98693 Ilmenau, Germany
7 State Key Laboratory of Superlattices and Microstructures, Institute of Semiconductors, Chinese Academy of Sciences, Beijing 100083, China
8 Beijing Academy of Quantum Information Science, Beijing 100193, China
9 Beijing Engineering Research Center of Semiconductor Micro-Nano Integrated Technology, Beijing 100083, China
* Correspondence: yanwei@semi.ac.cn (W.Y.); lizhaofeng@semi.ac.cn (Z.L.)

Abstract: We analyze the coupling between double nanowire cavities for both photonic modes and plasmonic modes. When the spacing between nanowires reduces, a redshift of the resonant frequency of the symmetric mode and a blueshift of the resonant frequency of the antisymmetric mode are observed. Compared to single nanowire cavity modes, the Q factors of antisymmetric supermodes of double nanowires can be improved by 51% for photonic modes and by 24% for plasmonic modes. The mechanisms of Q factor improvement for photonic modes and plasmonic modes are studied based on the field distribution of radiations from the modes. This paper may contribute to research and applications for double nanowire lasers and nanowire laser arrays.

Keywords: coupling; nanowire; photonic; plasmonic; cavity; Q factor; supermode; array

check for updates

Citation: Peng, X.; Liu, J.; Kang, Y.; Mao, X.; Yan, W.; Wang, X.; Liu, K.; Xu, R.; Yang, F.; Li, Z. Coupling of Photonic and Plasmonic Modes for Double Nanowire Cavities. *Photonics* **2023**, *10*, 415. https://doi.org/10.3390/photonics10040415

Received: 14 March 2023
Revised: 3 April 2023
Accepted: 4 April 2023
Published: 6 April 2023

1. Introduction

To achieve photonic integrated circuits (PICs), nanoscale lasers have seen great development in the past two decades. Various designs were brought up in pursuit of properties, including ultracompact footprints, low thresholds, and room-temperature operation [1–3]. However, influences between multiple devices must be taken into account in more practical applications, which encouraged studies towards nano-laser arrays, including both coupled and uncoupled arrays [4]. In this area, arrays consisting of two nano-lasers are essential as a building block toward more complex arrays of nano-lasers.

A large number of studies focused on mode splitting, which is a universal phenomenon in coupled resonators such as nanoscale rings, nanopans, and square standing-wave cavity resonators [5–7]. Both coupled metallo-dielectric cylinder nanocavities [8] and coupled photonic crystal nanolasers [9] could create supermodes. Some of the studies aimed at mode selection and switching [10], while some other studies aimed to curb coupling [8,11]. The coupling between nanowires has been studied in previous research, for both aligned and parallel nanowires [12]. However, a few studies have been conducted regarding coupled modes of double nanowire cavities (DNC), both in photonic and plasmonic modes.

In fact, nanowire lasers have attracted great interest as the principal kind of nanoscale lasers [13–16]. Semiconductor nanowire acts simultaneously as an optical gain medium and an optical cavity that, in some cases, possesses the intrinsic capability to produce laser light [17]. Nanowire cavities have also manifested outstanding properties in many other aspects [18–21]. Nanowire lasers also enable wavelength multiplexing and potential electrical modulation for on-chip applications [22]. However, such lasers are restricted by the diffraction limit, both in optical mode size and physical device dimension [23].

Surface plasmon polariton (SPP) is a kind of coherent electron oscillation at metal-dielectric interfaces [24]. Electromagnetic (EM) fields of surface plasmons decrease exponentially away from the interface, which allows lightwaves to be concentrated at sub-diffraction limit scales [25]. The interaction between SPPs and exciton has been studied both in weak coupling and strong coupling [26]. Exploiting this mechanism, plasmonic lasers (or spasers) of the nanoscale have been realized based on core-shell silica nanoparticles [27], metal-coated dielectric nanowires [28], silver nanopans [29], metal-insulator-metal waveguides [30], metal-insulator-semiconductor nanowire [23], and methylene blue dye-Ag nanocavities [31,32]. Among the above plasmonic lasers, nanowire plasmonic lasers [23,24,33–37] play an important role. Therefore, in this paper, coupled DNC is studied for both photonic modes and plasmonic modes.

In the following, finite element method (FEM) simulation results for photonic modes are presented, and the coupling effect on Q factors of different modes is discussed in Section 2. Then, in Section 3, the simulation results for plasmonic modes are shown and compared to those for photonic modes. Several topics related to the research results in the earlier sections are discussed subsequently in Section 4. Finally, Section 5 concludes the mechanisms in coupled DNC for photonic and plasmonic modes and discusses possible applications.

2. Coupling of Double Nanowire Cavities for Photonic Mode

The simulated DNCs are shown schematically in Figure 1a, consisting of two hybrid perovskite ($CH_3NH_3PbI_3$) semiconductor nanowires placed side by side with the spacing of S_1. Details of the parameters can be found in the caption of Figure 1. Hybrid perovskite ($CH_3NH_3PbI_3$) is chosen as the material of the nanowires in the present study based on previous reports [38,39]. In experiments, the synthesis of high-quality single-crystal perovskite can be achieved by a surface-initiated solution growth strategy [38]. The as-grown perovskite nanowires can be subsequently transferred onto the substrate to fabricate nanowire lasers [33].

It is worth noting that the main conclusions of the following results are not limited to the specific hybrid perovskite and still hold qualitatively for nanowire cavities of other dielectric materials. Since we mainly concentrate on the coupling of nanowire cavities, the substrate is not included in the simulation here for simplicity. The FEM software COMSOL Multiphysics is used in the simulation. Tetrahedron mesh is used. The minimum mesh size is 5 nm.

Single nanowire cavity (SNC) supports only fundamental modes (two degenerate modes polarized in the y and z directions) for wavelengths larger than 750 nm. When two identical nanowire cavities are placed side by side near each other, they support symmetric supermodes and antisymmetric supermodes (or bonding and antibonding modes). Symmetric modes and antisymmetric modes have similar or opposite EM field distributions, respectively, in two nanowire cavities. Figure 1b shows the E field profile on the y–z cross section for symmetric and antisymmetric modes of z and y polarizations. Figure 1c shows the symmetric and antisymmetric modes on the x–y cross section. Those symmetric and antisymmetric modes of z polarization are similar to the case of y polarization and are not shown here. In the following parts, the modes of y and z polarizations will be referred to as E_y modes and E_z modes, respectively.

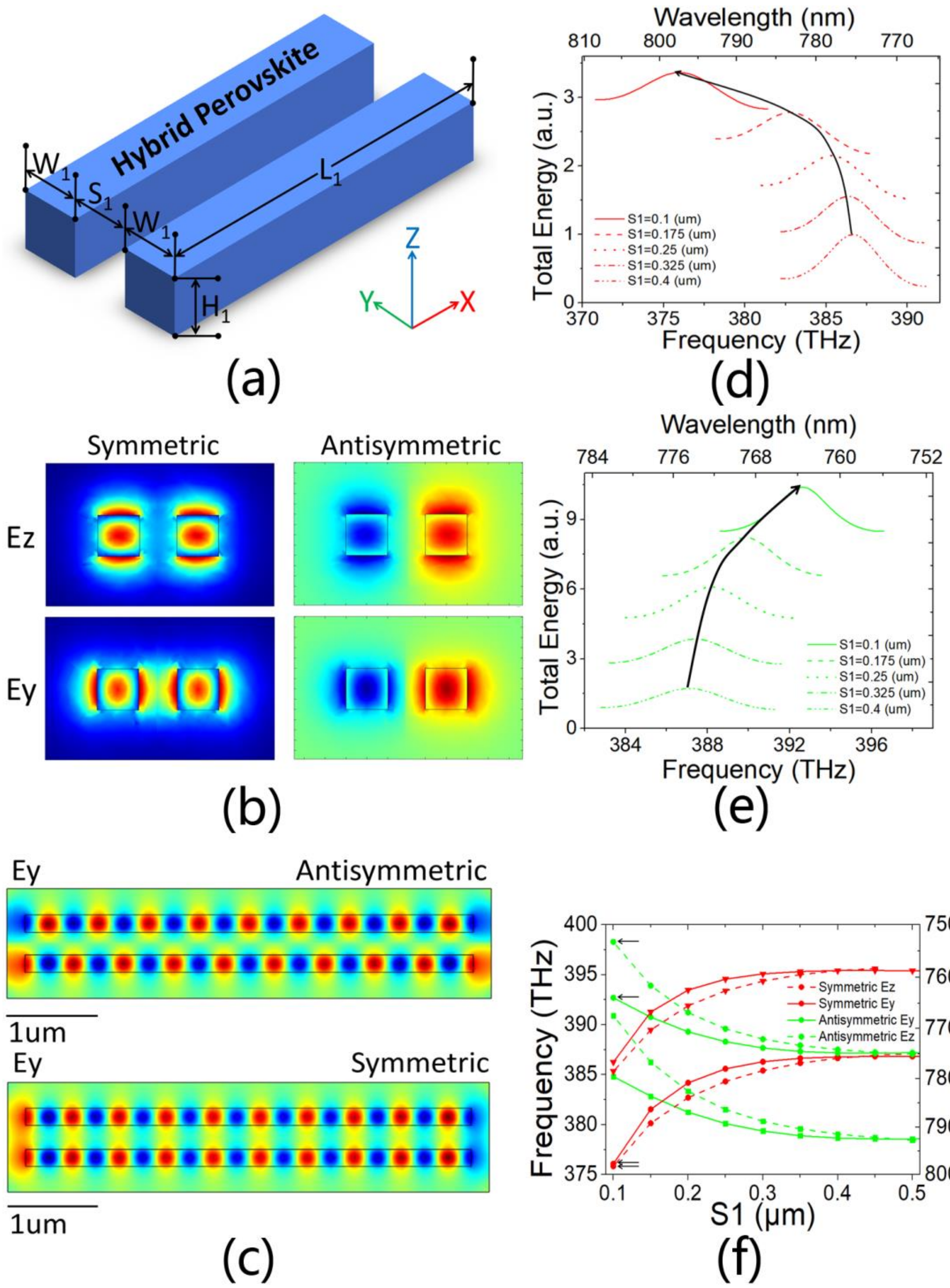

Figure 1. (**a**) Coupled photonic DNC. S_1 = 0.2 μm. L_1 = 5 um. $W_1 = H_1$ = 0.2 μm. The refractive index of semiconductor nanowire n = 2.59. The nanowires are placed in the air. (**b**) Electric field distribution at the y–z cross section of symmetric and antisymmetric modes of z and y polarizations. The z component of the E field is shown for E_z modes, while the y component of the E field is shown for E_y modes. (**c**) E field distribution at the x–y cross section for antisymmetric and symmetric E_y modes at the middle of the nanowire. The y component of the electric field is shown here, at frequencies of 380.3 and 385.4 THz, respectively. (**d**,**e**) Total energy spectra of symmetric E_y mode and antisymmetric E_y mode, respectively, as S_1 grows smaller. (**f**) Resonant frequencies versus S_1 for symmetric and antisymmetric modes of y and z polarizations.

To study the resonant modes, we calculate the total energy of the fields when the cavities are excited by short line sources for wavelengths between 750 nm and 800 nm. The peaks of the total energy spectra correspond to the resonant frequencies of modes. Figure 1d,e shows the shifting of spectra for symmetric and antisymmetric E_y modes when S_1 decreases from 0.4 μm to 0.1 μm. A redshift of the resonant frequency of the symmetric mode and a blueshift of the resonant frequency of the antisymmetric mode can be observed when S_1 decreases. The spectra for symmetric and antisymmetric E_z modes have the same tendency when S_1 decreases, but are not shown here. A series of resonant frequencies are plotted versus S_1 in Figure 1f.

To understand Figure 1f, we start with a single nanowire cavity. As a Fabry-Perot resonator, the longitudinal modes of SNC obey the following equation [40]:

$$\frac{1}{\lambda_{\text{eff}}^{q}} - \frac{1}{\lambda_{\text{eff}}^{q+1}} = \frac{1}{2L_1} \tag{1}$$

where q is a positive integer marking the longitudinal mode index; L_1 is the length of the Fabry-Perot resonator; λ_{eff} is the effective wavelength of the longitudinal mode. The effective wavelength λ_{eff} is calculated as $\lambda_{\text{eff}} = 2\pi/\beta$, where β is the propagation constant of the longitudinal mode. The calculated effective wavelengths of the longitudinal modes agree well with Equation (1). For SNC, which has a square cross section, longitudinal modes are two-fold degenerate in y and z polarizations. When two nanowires are placed far away from each other, they resonate just as two independent SNCs. When the two nanowires are placed near each other, the two degenerate modes of the same q index will split into four nondegenerate modes (two E_y supermodes and two E_z supermodes for DNC), as shown in Figure 1f. For instance, when S_1 = 0.5 μm, four supermodes with frequencies near 387.1 THz originate from the coupling of the two degenerate longitudinal modes of SNC. When S_1 decreases, the frequencies of the four modes split, i.e., the redshift of symmetric modes and the blueshift of antisymmetric modes. The same phenomenon also happens in other longitudinal modes (378.6 THz and 395.3 THz). Four supermodes that originate at 387.1 THz are depicted for clarity in Figure 1f, but only two antisymmetric supermodes that originate at 378.6 THz and two symmetric supermodes that originate at 395.3 THz are presented.

From Figure 1f, it is also seen that the difference between the resonant frequencies of symmetric and antisymmetric modes increases when S_1 decreases. This phenomenon was named "mode splitting" [5–7]. Due to the redshift and blueshift of resonant frequencies for symmetric and antisymmetric modes, the curves of frequency tendency from neighboring longitudinal modes can intersect, and the resonant frequencies from neighboring longitudinal modes can overlap. This overlap could cause mode competition, which may not be desired in laser operation.

To further investigate the properties of the supermodes, total energy spectra are calculated for a longitudinal mode of SNC and four corresponding supermodes of DNC (Figure 2a). These four supermodes for S_1 = 0.1 μm of DNC are marked by arrows in Figure 1f. The quality factor (Q factor) for these modes is calculated based on the full width at half maximum (FWHM) of the spectra. The Q factor of mode for SNC is 94.9. The Q factors of symmetric E_y and E_z modes for DNC are 68.7 and 83.2, respectively. The Q factors of the antisymmetric E_y and E_z modes for DNC are 133.2 and 143.1, respectively. Antisymmetric modes have higher Q factors than symmetric modes. This kind of Q factor splitting has been found in previous research on mode splitting [8]. Q factor splitting for E_z modes is stronger than Q factor splitting for E_y modes. Among the four supermodes, antisymmetric E_z mode has the highest Q factor. The Q factor of antisymmetric E_z mode for DNC is 51% higher than the Q factor for SNC mode.

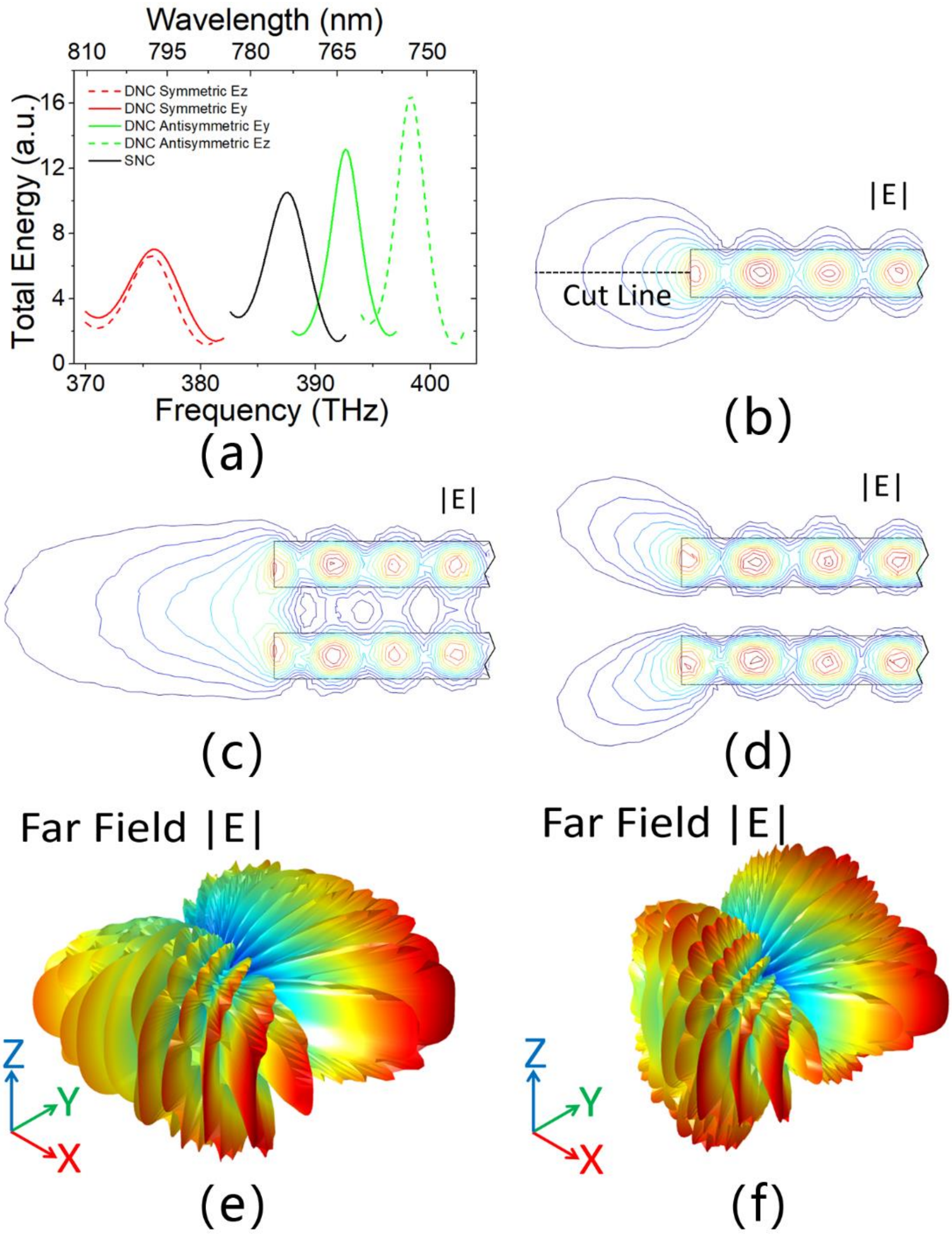

Figure 2. (**a**) Total energy spectra for the mode of SNC and corresponding four supermodes of DNC at S_1 = 0.1 um. Contour plot of the electric field norm for a longitudinal mode of SNC (**b**), symmetric E_z modes of (**c**), and antisymmetric E_z modes (**d**) for DNC at S_1 = 0.2 um. The lobe pattern of the electric field norm at the far field for antisymmetric E_y mode (**e**) and antisymmetric E_z mode (**f**) for DNC.

Different Q factors for symmetric and antisymmetric modes and two polarizations can be understood based on their radiation patterns. Firstly, we performed an analysis based on the symmetry property of supermodes. Figure 2b shows the radiation pattern of the mode of SNC, which is mainly along the direction of the longitudinal axis of the nanowire. Figure 2c shows the radiation pattern of the symmetric mode of DNC. The radiation is also mainly along the direction of the longitudinal axis of the DNC, which can be regarded as the constructive interference of two SNC modes. Figure 2d shows the radiation pattern of the antisymmetric modes of DNC. The radiation deviates from the direction of the longitudinal axis of the DNC. This radiation pattern can be regarded as the destructive interference of two SNC modes, which is similar to the radiation pattern of a quadrupole source. For clarity, Figure 2b–d shows only the radiation patterns around the left ends of the nanowires, while the patterns around the right ends are the same due to the symmetry of the structures. In comparison to SNC modes, destructive interference increases the Q factors of antisymmetric DNC modes. This is due to the reduced radiation energy of these modes.

Secondly, we analyze from the perspective of polarizations. For antisymmetric modes, E_z supermode has a higher Q factor than E_y supermode. To understand this phenomenon, the lobe patterns of radiation of E_y and E_z supermodes are plotted in Figure 2e,f. The difference between the EM far field distribution of two polarizations shows lower radiation energy for E_z supermode than radiation energy for E_y supermode. This explains the higher Q factors of antisymmetric E_z modes than those of antisymmetric E_y modes. Consequently, the antisymmetric E_z mode has the highest Q factor among the four supermodes.

3. Coupling of Double Nanowire Cavities for Plasmonic Mode

In the simulation for coupled plasmonic DNC, a metallic (Ag) substrate is introduced below two hybrid perovskite semiconductor nanowires placed side by side (Figure 3a). The relative permittivity of the metallic substrate is fitted with the Drude–Lorentz dispersion model (high-frequency dielectric constant $\varepsilon_\infty = 3.75$, plasma frequency $\omega_p = 1.32 \times 10^{16}$ rad/s, characteristic collision frequency $\gamma = 1.20 \times 10^{14}$ rad/s).

Plasmonic nanowire lasers work similarly to photonic nanowire lasers in some aspects and thus have similar phenomena in the coupled DNC system. A distinction between photonic modes and plasmonic modes is the EM field distribution. The EM field for plasmonic modes exists mainly at the interface between metal and dielectric and attenuates exponentially vertically (Figure 3b). Contrastively, the EM field for photonic modes lies mainly in the central area of the cavity (Figure 1b), especially for fundamental modes. Moreover, only TM mode (or E_z mode) exists in plasmonic modes, contrasting with E_z and E_y modes in photonic modes.

Symmetric modes and antisymmetric modes of plasmonic DNC can be observed, as shown in Figure 3b. Resonant frequencies of supermodes versus S_2 are plotted in Figure 3c,d for $L_2 = 5$ μm and $L_2 = 3$ μm, respectively, which indicates the mode splitting of plasmonic DNC. The longitudinal modes of plasmonic SNC split into two supermodes of plasmonic DNC when two identical nanowires are placed near each other. The longitudinal spacings are smaller for modes of relatively longer DNCs, as shown in Figure 3c. And the overlap of mode frequencies happens earlier when S_2 decreases. This overlap still exists even when the nanowires are as short as 3 μm for plasmonic DNC, as shown in Figure 3d. Figure 3c, similar to Figure 1f, illustrates simply the antisymmetric supermode at 384.9 THz and the symmetric supermode at 397.1 THz, for the sake of clarity. For the same reason, only the antisymmetric supermode, which originates at 376.1 THz, and the symmetric supermode, which originates at 406.8 THz, are demonstrated here in Figure 3d.

A longitudinal mode of plasmonic SNC and two supermodes of plasmonic DNC are used to calculate their total energy spectra (Figure 3e). These two supermodes for $S_2 =$ 0.1 μm of plasmonic DNC are marked by arrows in Figure 3d. The Q factor of mode for SNC is 59.6. The Q factors of symmetric mode and antisymmetric mode for DNC are 58.5 and 75, respectively. These results exhibit the Q factor splitting of coupled plasmonic DNC. Q factors for antisymmetric modes are higher than symmetric modes of plasmonic DNC. The mechanism of different Q factors for modes of plasmonic DNC is similar to that of photonic DNC, i.e., destructive interference and constructive interference.

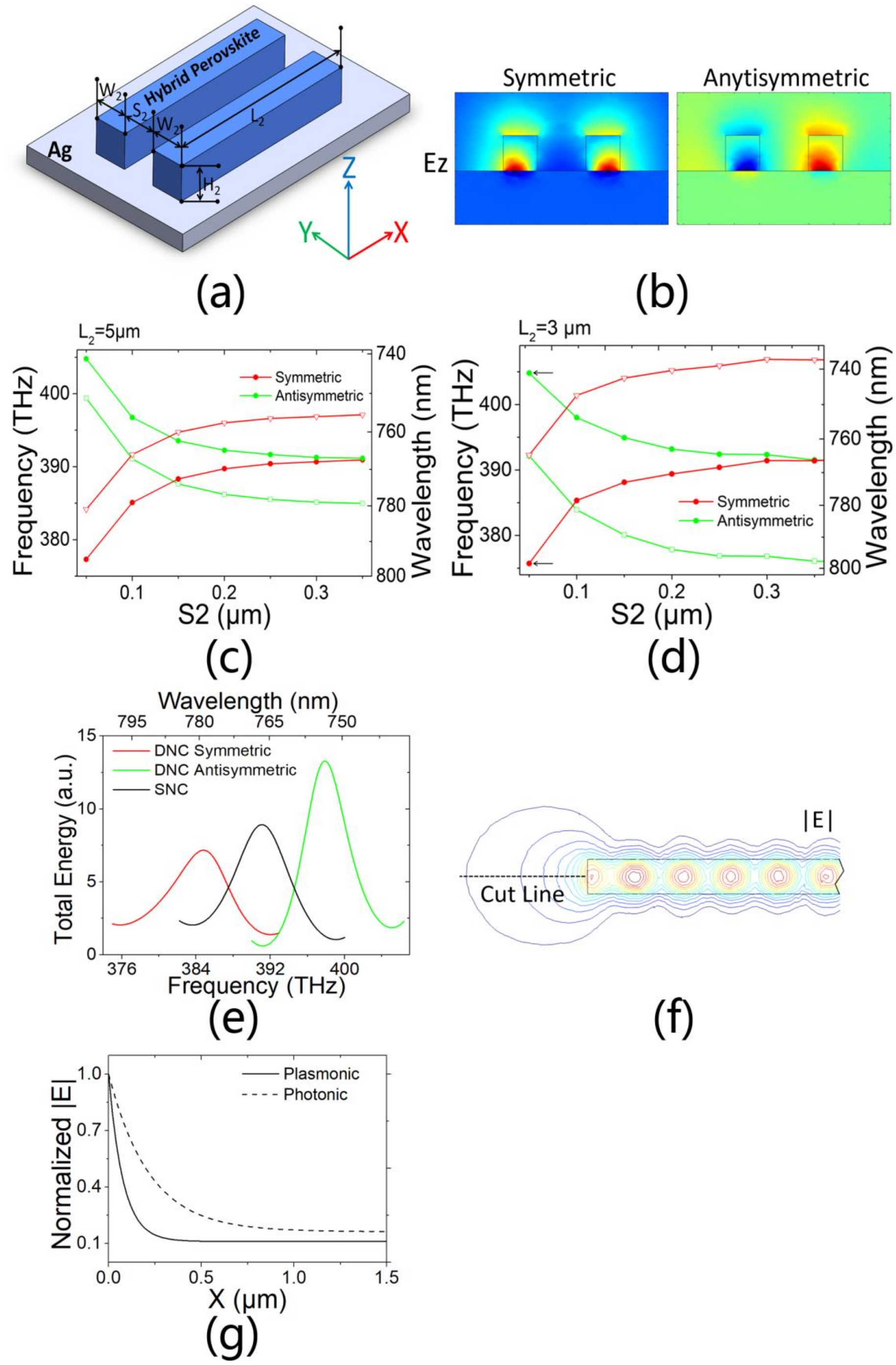

Figure 3. (**a**) Coupled plasmonic DNC. S_2 = 0.2 mm. L_2 = 3 μm; W_2 = H_2 = 0.135 mm. The refractive index of hybrid perovskite semiconductor nanowire n = 2.59–0.015 i. The Ag substrate has parameters of ε_∞ = 3.75, $\omega_p = 1.32 \times 10^{16}$ rad/s, $\gamma = 1.20 \times 10^{14}$ rad/s. (**b**) E field distribution at y–z cross section of symmetric and antisymmetric modes. The z component of the E field is shown here. (**c**) Resonant frequencies of symmetric and antisymmetric modes versus S_2 when L_2 = 5 μm. (**d**) Resonant frequencies of symmetric and antisymmetric modes versus S_2 when L_2 = 3 μm. (**e**) Total energy spectra for mode of plasmonic SNC and corresponding two supermodes of plasmonic DNC with S_2 = 0.1 μm when L_2 = 3 μm. (**f**) Contour plot of the electric field norm for a longitudinal mode of plasmonic SNC. (**g**) Normalized electric field amplitudes versus distance from the ends of nanowires along the cut line (shown in (**f**) and Figure 2b) selected by main radiation directions for the mode of plasmonic SNC (line) and the mode of photonic SNC (dash).

The Q factor of the antisymmetric mode of plasmonic DNC has an improvement of up to 24% over the Q factor of the mode of plasmonic SNC. This improvement in the Q factor is lower compared with the result (51%) for the case of photonic modes in Section 3. This different improvement of Q factors may be due to the different extents of destructive interference of antisymmetric modes of plasmonic DNC and photonic DNC. Additionally, the extent of interference from DNC is mainly determined by the radiation fields of SNC. The extent of the radiation fields of plasmonic SNC and photonic SNC is analyzed along the cut lines of the main radiation directions of modes as shown in Figures 3f and 2b, respectively. The normalized electric fields along the cut lines from the ends of nanowires are shown in Figure 3g, which demonstrates the attenuation of radiation fields away from the ends. The radiation electric field of plasmonic SNC attenuates faster than that of photonic SNC because of additional absorption loss due to the metallic substrate of plasmonic SNC. Consequently, the extent of interference in the antisymmetric mode of plasmonic DNC is smaller than that of photonic DNC. Moreover, the Q factor improvement in the case of plasmonic DNC is lower than that of photonic DNC.

4. Discussion

In Section 2, the substrate is excluded from the simulation for simplicity. In realistic applications, the presence of dielectric and metal substrates will affect the EM field distributions and Q factors of photonic modes. For instance, the Q factors of the photonic modes of DNC with SiO_2 substrate will decrease due to the effects of field delocalization and its displacement into the substrate, according to the simulation results. However, the main conclusions in Section 2, including longitudinal spacing, mode splitting, and Q factor splitting, are not influenced by the introduction of SiO_2 substrate.

However, the introduction of a metal (Ag) substrate will fundamentally change the question. For nanowires with a metal substrate, the supported modes are determined by the sizes of the cross section of nanowires with a certain refractive index for the studied wavelength band [33]. A nanowire with a height smaller than its critical value supports only the plasmonic modes [33]. When the height of the nanowire is larger than the critical value, both the plasmonic and hybrid modes will be supported. This hybrid mode is formed due to the hybridization of photonic modes and plasmonic modes [25,41,42]. According to this consideration, the dimensions of the plasmonic SNC and DNC in Section 3 are designed to support only the plasmonic modes, excluding the hybrid modes.

Additionally, anisotropy might exist for single-crystal perovskite nanowires [43]. However, the anisotropy of the material is not decisive for the main conclusions of this study. When the anisotropy is not crucial for the physical phenomena, the use of a scalar refractive index is acceptable, as has been done in other studies [38,44–46]. Therefore, the real part of the refractive index is set at $n = 2.59$ in our study based on previous research on $CH_3NH_3PbI_3$ [39]. The imaginary part of the refractive index is set at $k = -0.015$ to introduce an appropriate gain in the nanowire to compensate for the absorption loss due to the metallic substrate. This k corresponds to a gain level for laser physics 2.7×10^3 cm^{-1}, which is within the realizable gain level of perovskite in previous studies [47]. With this gain level, the intensity of the mode will remain approximately constant when it propagates in the nanowire.

5. Conclusions

The coupling of DNC is studied in this paper for both photonic modes and plasmonic modes. Our results revealed a mode splitting. A longitudinal mode of photonic SNC splits into four supermodes of photonic DNC. Moreover, a longitudinal mode of plasmonic SNC splits into two supermodes of plasmonic DNC. Due to the redshift and blueshift of resonant frequencies for symmetric and antisymmetric supermodes, the resonant frequencies of supermodes from neighboring longitudinal modes of DNC can overlap. This overlap of mode frequencies still exists even when the nanowires are as short as 3 μm for plasmonic

DNC. The possible overlap of frequencies of longitudinal modes should be taken into account when DNC or nanowire laser arrays are designed.

The Q factors of antisymmetric modes of DNC are higher than the Q factors of modes of SNC, for both photonic and plasmonic modes. The reason is that the antisymmetric modes have lower radiation loss due to the destructive interference of radiation from two SNCs. However, this improvement in Q factors for plasmonic modes (24%) is lower than that for photonic modes (51%). This difference can be explained by the faster attenuation of the radiation field for plasmonic modes than for photonic modes. The improvement of Q factors in DNC may be applied to improve nanowire lasers.

Author Contributions: Conceptualization, X.P. and Z.L.; validation, X.P. and J.L.; writing—original draft preparation, X.P. and Z.L.; writing—review and editing, J.L. and Y.K.; visualization, X.P.; supervision, Z.L.; project administration, X.M., W.Y. and R.X.; funding acquisition, X.W., K.L., F.Y. and Z.L. All authors have read and agreed to the published version of the manuscript.

Funding: This work was mostly supported by the National Key R&D Program of China (2018YFE0204000) and partially supported by the National Natural Science Foundation of China (Grant No. 61971395).

Institutional Review Board Statement: Not applicable.

Informed Consent Statement: Not applicable.

Data Availability Statement: Not applicable.

Conflicts of Interest: The authors declare no conflict of interest.

References

1. Gu, Q.; Smalley, J.S.T.; Nezhad, M.P.; Simic, A.; Lee, J.H.; Katz, M.; Bondarenko, O.; Slutsky, B.; Mizrahi, A.; Lomakin, V.; et al. Subwavelength semiconductor lasers for dense chip-scale integration. *Adv. Opt. Photonics* **2014**, *6*, 1–56. [CrossRef]
2. Hill, M.T.; Gather, M.C. Advances in small lasers. *Nat. Photonics* **2014**, *8*, 908–918. [CrossRef]
3. Ma, R.M.; Oulton, R.F. Applications of nanolasers. *Nat. Nanotechnol.* **2019**, *14*, 12–22. [CrossRef]
4. Deka, S.S.; Jiang, S.Z.; Pan, S.H.; Fainman, Y. Nanolaser arrays: Toward application-driven dense integration. *Nanophotonics* **2021**, *10*, 149–169. [CrossRef]
5. Haus, H.A.; Huang, W.P. Coupled-mode theory. *Proc. IEEE* **1991**, *79*, 1505–1518. [CrossRef]
6. Li, Q.; Wang, T.; Su, Y.K.; Yan, M.; Qiu, M. Coupled mode theory analysis of mode-splitting in coupled cavity system. *Opt. Express* **2010**, *18*, 8367–8382. [CrossRef]
7. Popovic, M.A.; Manolatou, C.; Watts, M.R. Coupling-induced resonance frequency shifts in coupled dielectric multi-cavity filters. *Opt. Express* **2006**, *14*, 1208–1222. [CrossRef]
8. Deka, S.S.; Pan, S.H.; Gu, Q.; Fainman, Y.; El Amili, A. Coupling in a dual metallo-dielectric nanolaser system. *Opt. Lett.* **2017**, *42*, 4760–4763. [CrossRef] [PubMed]
9. Hamel, P.; Haddadi, S.; Raineri, F.; Monnier, P.; Beaudoin, G.; Sagnes, I.; Levenson, A.; Yacomotti, A.M. Spontaneous mirror-symmetry breaking in coupled photonic-crystal nanolasers. *Nat. Photonics* **2015**, *9*, 311–315. [CrossRef]
10. Haddadi, S.; Hamel, P.; Beaudoin, G.; Sagnes, I.; Sauvan, C.; Lalanne, P.; Levenson, J.A.; Yacomotti, A.M. Photonic molecules: Tailoring the coupling strength and sign. *Opt. Express* **2014**, *22*, 12359–12368. [CrossRef]
11. Atlasov, K.A.; Karlsson, K.F.; Rudra, A.; Dwir, B.; Kapon, E. Wavelength and loss splitting in directly coupled photonic-crystal defect microcavities. *Opt. Express* **2008**, *16*, 16255–16264. [CrossRef] [PubMed]
12. Anikina, M.A.; Roy, P.; Kadinskaya, S.A.; Kuznetsov, A.; Kondratev, V.M.; Bolshakov, A.D. Numerical Study of GaP Nanowires: Individual and Coupled Optical Waveguides and Resonant Phenomena. *Nanomaterials* **2023**, *13*, 56. [CrossRef] [PubMed]
13. Huang, M.H.; Mao, S.; Feick, H.; Yan, H.Q.; Wu, Y.Y.; Kind, H.; Weber, E.; Russo, R.; Yang, P.D. Room-temperature ultraviolet nanowire nanolasers. *Science* **2001**, *292*, 1897–1899. [CrossRef]
14. Johnson, J.C.; Choi, H.J.; Knutsen, K.P.; Schaller, R.D.; Yang, P.D.; Saykally, R.J. Single gallium nitride nanowire lasers. *Nat. Mater.* **2002**, *1*, 106–110. [CrossRef]
15. Johnson, J.C.; Yan, H.Q.; Schaller, R.D.; Haber, L.H.; Saykally, R.J.; Yang, P.D. Single nanowire lasers. *J. Phys. Chem. B* **2001**, *105*, 11387–11390. [CrossRef]
16. Zimmler, M.A.; Capasso, F.; Muller, S.; Ronning, C. Optically pumped nanowire lasers: Invited review. *Semicond. Sci. Technol.* **2010**, *25*, 12. [CrossRef]
17. Eaton, S.W.; Fu, A.; Wong, A.B.; Ning, C.Z.; Yang, P.D. Semiconductor nanowire lasers. *Nat. Rev. Mater.* **2016**, *1*, 11. [CrossRef]
18. Kotal, S.; Artioli, A.; Wang, Y.J.; Osterkryger, A.D.; Finazzer, M.; Fons, R.; Genuist, Y.; Bleuse, J.; Gerard, J.M.; Gregersen, N.; et al. A nanowire optical nanocavity for broadband enhancement of spontaneous emission. *Appl. Phys. Lett.* **2021**, *118*, 6. [CrossRef]

19. Kuznetsov, A.; Roy, P.; Grudinin, D.V.; Kondratev, V.M.; Kadinskaya, S.A.; Vorobyev, A.A.; Kotlyar, K.P.; Ubyivovk, E.V.; Fedorov, V.V.; Cirlin, G.E.; et al. Self-assembled photonic structure: A Ga optical antenna on GaP nanowires. *Nanoscale* **2023**, *15*, 2332–2339. [CrossRef]
20. Roy, P.; Bolshakov, A.D. Ga-GaP nanowire hybrid optical system for enhanced coupling, focusing and steering of light. *J. Phys. D-Appl. Phys.* **2020**, *53*, 8. [CrossRef]
21. Zhang, G.Q.; Takiguchi, M.; Tateno, K.; Tawara, T.; Notomi, M.; Gotoh, H. Telecom-band lasing in single InP/InAs heterostructure nanowires at room temperature. *Sci. Adv.* **2019**, *5*, 8. [CrossRef] [PubMed]
22. Wang, D.Q.; Wang, W.J.; Knudson, M.P.; Schatz, G.C.; Odom, T.W. Structural Engineering in Plasmon Nanolasers. *Chem. Rev.* **2018**, *118*, 2865–2881. [CrossRef]
23. Oulton, R.F.; Sorger, V.J.; Zentgraf, T.; Ma, R.M.; Gladden, C.; Dai, L.; Bartal, G.; Zhang, X. Plasmon lasers at deep subwavelength scale. *Nature* **2009**, *461*, 629–632. [CrossRef]
24. Lv, Y.C.; Xu, F.F.; Wang, K.; Li, Y.J.; Zhao, Y.S. Loss compensation of surface plasmon polaritons in organic/metal nanowire heterostructures toward photonic logic processing. *Sci. China-Mater.* **2020**, *63*, 1464–1471. [CrossRef]
25. Balykin, V.I. Plasmon nanolaser: Current state and prospects. *Phys. Usp.* **2018**, *61*, 846–870. [CrossRef]
26. He, Z.; Xu, C.; He, W.; He, J.; Zhou, Y.; Li, F. Principle and Applications of Multimode Strong Coupling Based on Surface Plasmons. *Nanomaterials* **2022**, *12*, 1242. [CrossRef]
27. Noginov, M.A.; Zhu, G.; Belgrave, A.M.; Bakker, R.; Shalaev, V.M.; Narimanov, E.E.; Stout, S.; Herz, E.; Suteewong, T.; Wiesner, U. Demonstration of a spaser-based nanolaser. *Nature* **2009**, *460*, 1110–1112. [CrossRef] [PubMed]
28. Seo, M.K.; Kwon, S.H.; Ee, H.S.; Park, H.G. Full Three-Dimensional Subwavelength High-Q Surface-Plasmon-Polariton Cavity. *Nano Lett.* **2009**, *9*, 4078–4082. [CrossRef]
29. Kwon, S.H.; Kang, J.H.; Seassal, C.; Kim, S.K.; Regreny, P.; Lee, Y.H.; Lieber, C.M.; Park, H.G. Subwavelength Plasmonic Lasing from a Semiconductor Nanodisk with Silver Nanopan Cavity. *Nano Lett.* **2010**, *10*, 3679–3683. [CrossRef]
30. Hill, M.T.; Marell, M.; Leong, E.S.P.; Smalbrugge, B.; Zhu, Y.C.; Sun, M.H.; van Veldhoven, P.J.; Geluk, E.J.; Karouta, F.; Oei, Y.S.; et al. Lasing in metal-insulator-metal sub-wavelength plasmonic waveguides. *Opt. Express* **2009**, *17*, 11107–11112. [CrossRef] [PubMed]
31. Han, X.; Li, F.; He, Z.; Liu, Y.; Hu, H.; Wang, K.; Lu, P. Double Rabi splitting in methylene blue dye-Ag nanocavity. *Nanophotonics* **2022**, *11*, 603–611. [CrossRef]
32. He, Z.C.; Li, F.; Zuo, P.; Xu, C.; He, W.H.; He, J.H.; Zhou, Y.P.; Zhang, Q.P.; Chen, K.; Huang, H.L.; et al. Strong Coupling in a Hybrid System of Silver Nanoparticles and J-Aggregates at Room Temperature. *J. Phys. Chem. C* **2022**, *126*, 17141–17151. [CrossRef]
33. Ren, K.K.; Wang, J.; Chen, S.Q.; Yang, Q.X.; Tian, J.; Yu, H.C.; Sun, M.F.; Zhu, X.J.; Yue, S.Z.; Sun, Y.; et al. Realization of Perovskite-Nanowire-Based Plasmonic Lasers Capable of Mode Modulation. *Laser Photon. Rev.* **2019**, *13*, 9. [CrossRef]
34. Sidiropoulos, T.P.H.; Roder, R.; Geburt, S.; Hess, O.; Maier, S.A.; Ronning, C.; Oulton, R.F. Ultrafast plasmonic nanowire lasers near the surface plasmon frequency. *Nat. Phys.* **2014**, *10*, 870–876. [CrossRef]
35. Yu, H.C.; Ren, K.K.; Wu, Q.; Wang, J.; Lin, J.; Wang, Z.J.; Xu, J.J.; Oulton, R.F.; Qu, S.C.; Jin, P. Organic-inorganic perovskite plasmonic nanowire lasers with a low threshold and a good thermal stability. *Nanoscale* **2016**, *8*, 19536–19540. [CrossRef] [PubMed]
36. Zhao, D.; Liu, W.; Zhu, G.B.; Zhang, Y.Y.; Wang, Y.C.; Zhou, W.Y.; Xu, C.X.; Xie, S.S.; Zou, B.S. Surface plasmons promoted single-mode polariton lasing in a subwavelength ZnO nanowire. *Nano Energy* **2020**, *78*, 10. [CrossRef]
37. Liu, Y.; Li, F.; Xu, C.; He, Z.; Gao, J.; Zhou, Y.; Xu, L. The Design and Research of a New Hybrid Surface Plasmonic Waveguide Nanolaser. *Materials* **2021**, *14*, 2230. [CrossRef]
38. Zhu, H.M.; Fu, Y.P.; Meng, F.; Wu, X.X.; Gong, Z.Z.; Ding, Q.; Gustafsson, M.V.; Trinh, M.T.; Jin, S.; Zhu, X.Y. Lead halide perovskite nanowire lasers with low lasing thresholds and high quality factors. *Nat. Mater.* **2015**, *14*, 636–642. [CrossRef]
39. Loper, P.; Stuckelberger, M.; Niesen, B.; Werner, J.; Filipic, M.; Moon, S.J.; Yum, J.H.; Topic, M.; De Wolf, S.; Ballif, C. Complex Refractive Index Spectra of CH3NH3PbI3 Perovskite Thin Films Determined by Spectroscopic Ellipsometry and Spectrophotometry. *J. Phys. Chem. Lett.* **2015**, *6*, 66–71. [CrossRef]
40. Yariv, A. *Photonics: Optical Electronics in Modern Communications*; Pub. House of Electronic: Hong Kong, China, 2007.
41. Goykhman, I.; Desiatov, B.; Levy, U. Experimental demonstration of locally oxidized hybrid silicon-plasmonic waveguide. *Appl. Phys. Lett.* **2010**, *97*, 3. [CrossRef]
42. Oulton, R.F.; Sorger, V.J.; Genov, D.A.; Pile, D.F.P.; Zhang, X. A hybrid plasmonic waveguide for subwavelength confinement and long-range propagation. *Nat. Photonics* **2008**, *2*, 496–500. [CrossRef]
43. Zhao, P.; Su, J.; Lin, Z.H.; Wang, J.P.; Zhang, J.C.; Hao, Y.; Ouyang, X.P.; Chang, J.J. The crystal anisotropy effect of MAPbI(3) perovskite on optoelectronic devices. *Mater. Today Energy* **2020**, *17*, 6. [CrossRef]
44. Chu, K.W.; Ma, F.Y.; Zhu, X.J.; Jia, X.H.; Huang, Z.T.; Dong, K.Q.; Sun, J.Q.; Liu, K.; Jin, P.; Wang, Z.J.; et al. Dimension-programmable CsPbBr3 nanowires for plasmonic lasing with PDMS templated technique. *J. Phys. D-Appl. Phys.* **2022**, *55*, 6. [CrossRef]
45. Jia, X.H.; Wang, J.; Huang, Z.T.; Chu, K.W.; Ren, K.K.; Sun, M.F.; Wang, Z.J.; Jin, P.; Liu, K.; Qu, S.C. Metallic cavity nanolasers at the visible wavelength based on in situ solution-grown Au-coated perovskite nanowires. *J. Mater. Chem. C* **2022**, *10*, 680–687. [CrossRef]

46. Singh, J.K.; Mandal, S.K.; Banerjee, G. Refractive index of different perovskite materials. *J. Mater. Res.* **2021**, *36*, 1773–1793. [CrossRef]
47. Sutherland, B.R.; Sargent, E.H. Perovskite photonic sources. *Nat. Photonics* **2016**, *10*, 295–302. [CrossRef]